Electronic Transport and Mechanical Properties of Phosphorus- and Phosphorus–Nitrogen-Doped Carbon Nanotubes

Eduardo Cruz-Silva,[†,‡,*] Florentino López-Urías,[†] Emilio Muñoz-Sandoval,[†] Bobby G. Sumpter,[‡] Humberto Terrones,[†] Jean-Christophe Charlier,[§] Vincent Meunier,[‡] and Mauricio Terrones[†]

[†]Laboratory for Nanoscience and Nanotechnology Research (LINAN) and Advanced Materials Department, IPICyT. Camino a la Presa Sn. Jose 2055, San Luis Potosí, Mexico, 78216, [‡]Oak Ridge National Laboratory, P.O. Box 2008, MS6367, Oak Ridge, Tennessee 37831-6367, and [§]Université Catholique de Louvain, PCPM & ETSF, Place Croix du Sud 1, B-1348 Louvain-la-Neuve, Belgium

ABSTRACT We present a density functional theory study of the electronic structure, quantum transport and mechanical properties of recently synthesized phosphorus (P) and phosphorus–nitrogen (PN) doped single-walled carbon nanotubes. The results demonstrate that substitutional P and PN doping creates localized electronic states that modify the electron transport properties by acting as scattering centers. Nonetheless, for low doping concentrations (1 doping site per ~200 atoms), the quantum conductance for metallic nanotubes is found to be only slightly reduced. The substitutional doping also alters the mechanical strength, leading to a 50% reduction in the elongation upon fracture, while Young's modulus remains approximately unchanged. Overall, the PN- and P-doped nanotubes display promising properties for components in composite materials and, in particular, for fast response and ultra sensitive sensors operating at the molecular level.

KEYWORDS: carbon nanotubes · doping · density functional theory · electronic transport · elastic properties

Uninterrupted scrutiny has accompanied carbon nanotube (CNT) research,[1,2] in large part thanks to outstanding structural, mechanical and electronic properties of the nanotubes—properties that make them good candidates for numerous applications as well as for the development of novel types of high performance functional materials. CNTs can behave as metals or semiconductors, depending on their particular geometry,[3,4] and abundant new electronic applications have been devised.[5] Their unique mechanical properties also make them very appealing as fillers in polymeric matrices to form new polymer nanocomposite materials.[6] However the tremendous promise as fundamental building blocks of nanocomposites and nanoelectronic devices has not been fully realized. This is in part due to the lack of control of the reactivity of the outer CNT walls. The doping of carbon nanotubes offers a practical path to tailor their physical and chemical properties by creating new states that modify their electronic structure. The presence of these states originates from the different electronic configurations of the doping atoms. These modifications in the electronic structure and surface reactivity can help to achieve significantly improved materials, and new applications of doped carbon nanotubes have emerged, such as enhanced field emission,[7] fuel cell electrodes,[8] support for catalytic particles,[9,10] and protein immobilization.[11]

Doping can be achieved by intercalation, encapsulation, and substitution.[12] Nitrogen and boron are among the most studied substitutional dopants used in nanotube research.[13] In recent works[14,15] we reported the successful experimental phosphorus (P) and phosphorus–nitrogen (PN) heteroatomic doping of carbon nanotubes by thermolysis of mixtures of ferrocene and triphenyl phosphine (TPP) dissolved in benzylamine[14] and ethanol.[15] In this account, we present new results that provide a better understanding of the phosphorus binding to the nanotube lattice and its effects on the nanotube properties. In particular, we have investigated the electronic structure and the energetics of P- and PN-doped graphene and carbon nanotubes, as well as the effects of doping on their mechanical strength. In addition, electron transport calculations provide valuable information regarding the possible use of these doped nanotubes as efficient molecular sensors.

*Address correspondence to cruzsilvae@ornl.gov.

Received for review March 23, 2009 and accepted June 17, 2009.

Published online July 2, 2009.
10.1021/nn900286h CCC: $40.75

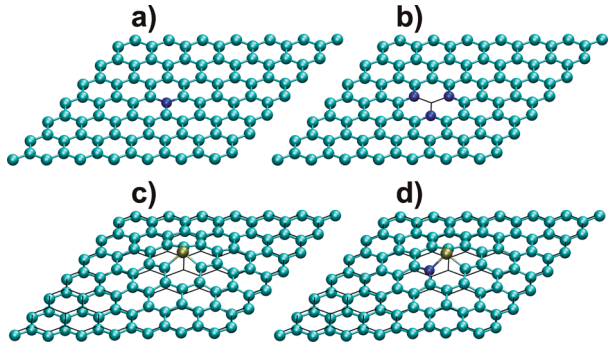

Figure 1. Relaxed structures of graphene, doped with (a) nitrogen, (b) N_3 pyridinic-like doping, (c) phosphorus, and (d) phosphorus−nitrogen. The pristine carbon positions are represented with a black hexagonal network. It can be observed that the presence of phosphorus induces great stress and corrugation in graphene.

RESULTS AND DISCUSSION

Graphene (single-layered graphite) constitutes a reasonable model for evaluating the behavior of the limiting case of large diameter nanotubes. Therefore, we used graphene to investigate the plausibility of doping large diameter nanotubes with P, as well as PN systems, and for describing as realistically as possible the experimental results on doping of MWCNTs[14] and SWNTs.[15]

Pristine and N-doped graphene were taken as references. The reason is that low concentration of substitutional nitrogen doping does not cause major distortions in graphene, as can be observed from Figure 1a. The C−N bond length is less than 2% shorter than the C−C bond, and first- and second-neighbors only experience small displacements (less than 0.7% change in their bond lengths) to compensate for this shortening. This is true also for N_3 pyridinic-like doping of graphene (Figure 1b), but with a vacancy created in the center of the defect. However, doping with phosphorus (with or without nitrogen) causes significantly larger distortions in graphene (Figure 1c,d). Phosphorus preserves its sp^3 character, and bonds with tetrahedral-like configurations, with bond angles close to 99°. The P−C bond length is 1.79 Å, which is quite large compared to 1.42 Å for C−C sp^2 bonds. The 26% increase in the bond length combined with the difference in bond angles, forces P to protrude from the graphene plane, displacing also the positions of the first-, second-, and third-neighbors out of the plane (see Figure 1c). This can be interpreted as a corrugation induced by the presence of P atoms. For PN-doped graphene (see Figure 1d), the presence of nitrogen helps to reduce the displacements caused by the inclusion of phosphorus, thus resulting in a "damping" effect on the structural strain, especially within the shells of first- and second-neighbors. This effect can be quantified by analyzing the total energy calculations (Table 1). The defect formation energy was calculated in the following way. First, the binding energy of the complete supercell was calculated as defined in the following equation:

$$E_{B-SC}=(N_C E_C + N_N E_N + N_P E_P) - E_{total} \quad (1)$$

where E_{B-SC} is the binding energy of the supercell, E_{Total} is the total energy of the supercell, N_X is the number of atoms of the element X and E_X is the total energy of an isolated atom of the element X.

The defect energy is calculated by the difference of the supercell binding energy for each doped system with the undoped graphene, as shown on eq 2. The N3-vacancy system is special, because an atom is missing. In this case, the binding energy of the graphene supercell is scaled to reflect the difference in the number of atoms.

$$E_{defect} = E_{B\text{-pristine}} - E_{B\text{-doped}} \quad (2)$$

Table 1 summarizes the results for the different systems. Even though the P-doped systems have high defect-formation energies, these are comparable to the N_3-vacancy formation energy. It is also noted that a single PN defect exhibits a lower formation energy (by ca. 0.45 eV) when compared to a single P defect. Consequently, the heteroatomic PN defect is more stable than the P defect in graphene and large nanotubes.

For nanotubes, the curved structure should help to reduce the strain needed to accommodate the larger phosphorus atoms. In the zigzag tube illustrated in Figure 2a, it can be observed that similar to the N-doped graphene, the bond lengths around the nitrogen atom are slightly shorter than for a pristine carbon nanotube, being 1.39 and 1.41 Å for the axial and diagonal directions, respectively, slightly smaller when compared to 1.43 and 1.44 Å for the pure carbon case. The nanotube does not suffer any major structural distortions, but there is a small reduction in the nanotube diameter at the defect site (7.97 Å at the defect sited *versus* 8.06 Å in the supercell boundary). Basically, the nitrogen atom moves inward from the nanotube wall by about 0.1 Å. The effects are similar for N_3 doped nanotubes, but in this case, the atom that is in the axial direction from the vacant site is bent inward, while the other two atoms are bent slightly outward from the nanotube surface.

For a phosphorus-doped (10,0) zigzag nanotube, the nonequivalent lengths for P−C bonds are 1.76 (axial) and 1.81 Å (diagonal), and it is clear that the phosphorus atom still tends to form sp^3 bonding and

TABLE 1. Formation Energy Associated with the Doping of a Graphene Layer, as Well as the Changes in Bond Length from the Doping Atom to Its First Neighbors. Energies Are Expressed in eV and Lengths in Å

system	defect energy	1st nn bond A	1st nn bond B
pristine	—	1.42	1.42
N-doped	0.732	1.39	1.39
N_3-doped	4.423	1.33	1.33
P-doped	6.637	1.78	1.78
PN-doped	6.180	1.78	1.80

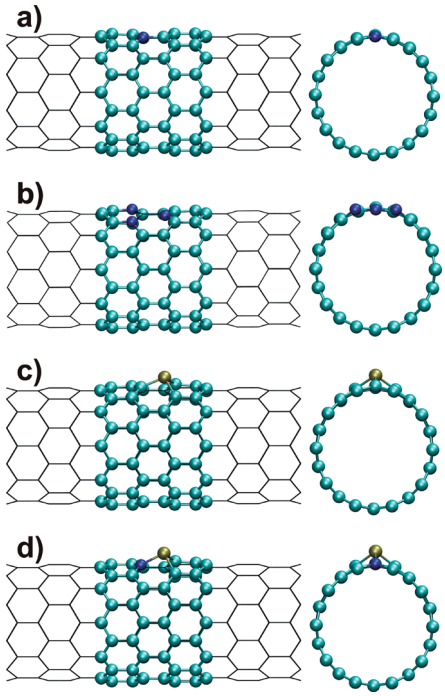

Figure 2. Relaxed structures of relaxed (10,0) armchair nanotube, doped with (a) nitrogen, (b) N_3 pyridinic like doping, (c) phosphorus, and (d) phosphorus−nitrogen. The position of phosphorus atom protrudes from the nanotube wall due to the longer P−C bonds.

assumes a trigonal pyramidal coordination (see Figure 2b). However, in the present case, the curved nanotube structure helps to reduce the strain needed to accommodate the phosphorus impurity. The distortion of the hexagonal network is primarily limited to the first-neighbors, with only a small displacement for the second-neighbors, while the third-neighbors are virtually unaffected. In addition, the shape of the cross-section of the nanotube changes from circular to slightly oval, with diameters of 7.8 (minor) and 8.28 Å (major, measured at the first neighbors of defect). The tube diameter at the defect site is 8.99 Å, and the phosphorus atom protrudes outwardly from the nanotube wall.

The PN-doped (10,0) nanotube has very similar features to that of the P-doped case (see Figure 2c). In particular, the phosphorus still prefers the sp^3 bonding. However for PN doping, the nitrogen atom helps to reduce the strain in the carbon network. Although the P atom displacement from its ideal position in the network is increased, the displacement of the surrounding atoms is reduced.

The structural effects of doping of the metallic armchair (6,6) nanotube, are very similar to that of a zigzag nanotube: the C−N bonds are shorter than the C−C bonds observed in pristine nanotubes, being 1.40 Å in both diagonal and tangential directions, compared to 1.43 Å in the pristine nanotube. Similar to the zigzag case, the nitrogen atom bends inwardly from the nanotube surface. The nanotube diameter at the nitrogen

TABLE 2. Formation Energy Associated with the Doping of (10,0) and (6,6) Nanotube, And the Changes in Bond Length from the Doping Atom to Its First Neighbors A and B. Energies Are Expressed in eV and Lengths in Å

system	defect energy	bond A	bond B
pristine (10,0)	—	1.43	1.44
N-doped (10,0)	0.933	1.39	1.41
N_3-doped (10,0)	4.015	1.33	1.34
P-doped (10,0)	5.553	1.76	1.81
PN-doped (10,0)	5.412	1.77	1.83
pristine (6,6)	—	1.44	1.43
N-doped (6,6)	0.737	1.40	1.40
N_3-doped (6,6)	3.766	1.33	1.34
P-doped (6,6)	5.578	1.82	1.78
PN-doped (6,6)	5.410	1.84	1.79

site is 8.20 Å, compared to 8.30 Å in the boundary of the supercell. For the N_3 doped (6,6) nanotube, we observe again an uneven bending of the atoms positions. In this case, the nitrogen atom that is in the tangential direction of the vacant site is pushed outward from the surface, while the other two atoms, closer to the axial direction, remain at the tube surface.

For the P-doped (6,6) nanotube, the bond lengths are 1.78 Å for the diagonal and 1.82 Å for the tangential bonds, while the angles are still very close to the 98° angle that phosphorus adopts in triphenyl phosphine. For the PN case, the structure is also very similar to that observed in the zigzag nanotube. As mentioned earlier, the nitrogen atom clearly helps to reduce the structural strain caused by the phosphorus impurity.

In a previous work, we showed that nitrogen doping in SWNTs leads to an increase in the corrugation of nanotube walls and the promotion of tube closure, which in turn could lead to the appearance of bamboo-type structures.[16] It is expected that higher levels of PN doping will have major effects in the carbon nanotube structure. Also, the limitations imposed by the periodicity of the model and the small amount of atoms prevent us from observing effects such as the formation of caps or bamboo-like walls. The thermal stability of all substitutionally doped nanotubes systems was verified using quantum molecular dynamics at a temperature of 1000 K and for times up to 1 picosecond.

Total energy and electronic structure calculations were performed on these nanotubes and the defect formation energies have been calculated using eqs 1−2, and summarized in Table 2. It is noteworthy that the formation energies for P and PN defects embedded in narrow diameter nanotubes are reduced by 1 and 0.7 eV, respectively, when compared to graphene. This indicates again that curvature helps to reduce the strain in the nanotubes after the phosphorus insertion. It is also important to notice that the difference in energy of P and PN defects is reduced from 0.45 eV in graphene to about 0.15 eV in nanotubes, highlighting the strain-

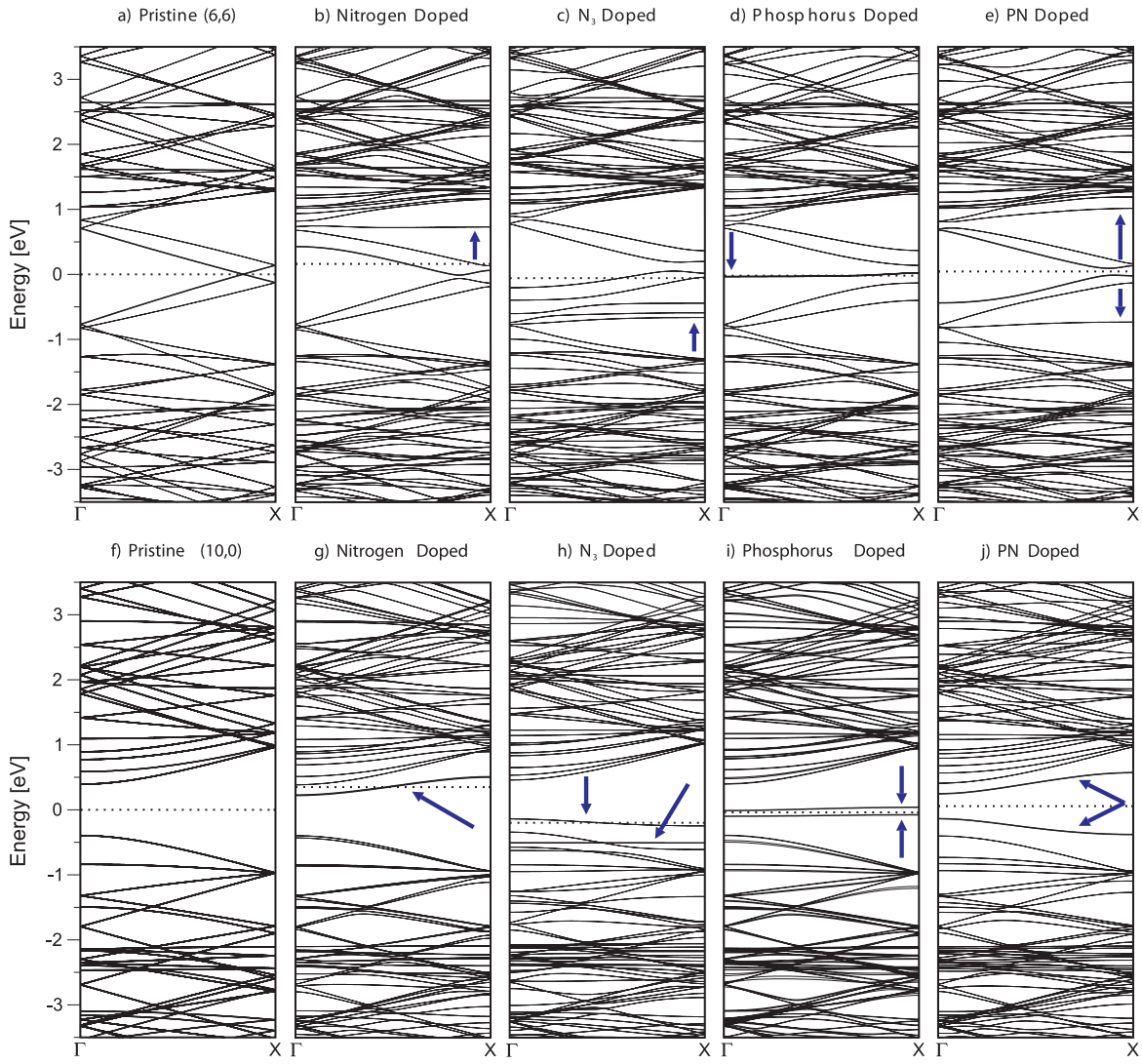

Figure 3. Band structure of pristine and doped (6,6) armchair metallic nanotubes (top) and (10,0) zigzag semiconducting nanotubes (bottom): (a,f) pristine, (b,g) nitrogen doped, (c,h) N_3 doped, (d,i) phosphorus doped, and (e,j) phosphorus−nitrogen doped. The presence of localized states around the defects is reflected as the low dispersion bands indicated by arrows. Notice that in the phosphorus-doped cases, the bands are dispersionless, indicating strong localization.

reducing property of the curvature, as well as the "damping" role played by nitrogen in graphene.

The band structures for pristine (6,6) and (10,0) carbon nanotubes are presented in Figure 3a−f. Substitutional doping with nitrogen induces new electronic states, as depicted in the band structure plots of Figure 3b,g, and indicated by blue arrows. For the metallic (6,6) nanotube (Figure 3b), the state related to the presence of N appears in the conduction bands, and the extra electron from nitrogen is injected into the conduction bands. In the case of the (10,0) semiconducting nanotube, the state created (Figure 3g) lies beneath the conduction bands and is occupied by one electron (the extra electron from nitrogen). It follows that the Fermi energy (indicated by the dotted line) in the nanotube is shifted close to the conduction bands, causing all nitrogen-doped semiconducting nanotubes to be metallic, the doping being of *n*-type, that is, the majority carriers are electrons. Pyridinic-like nitrogen doping of carbon nanotubes (Figure 3c,h) has a different effect, creating localized states in the valence bands, and shifting the Fermi level to their domain, that is, they behave as a *p*-type semiconductor.

Phosphorus also has five electrons in its valence shell, but it bonds with sp^3 hybridization, following a

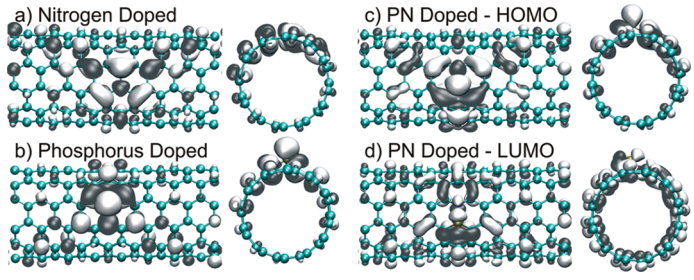

Figure 4. Representation of the wave functions, plotted at the isosurface of ±0.05 $Å^{-3/2}$: (a) nitrogen-doped nanotube top valence band, (b) phosphorus-doped nanotube top valence band; (c) phosphorus−nitrogen-doped nanotube top valence band, and (d) lowest conduction band.

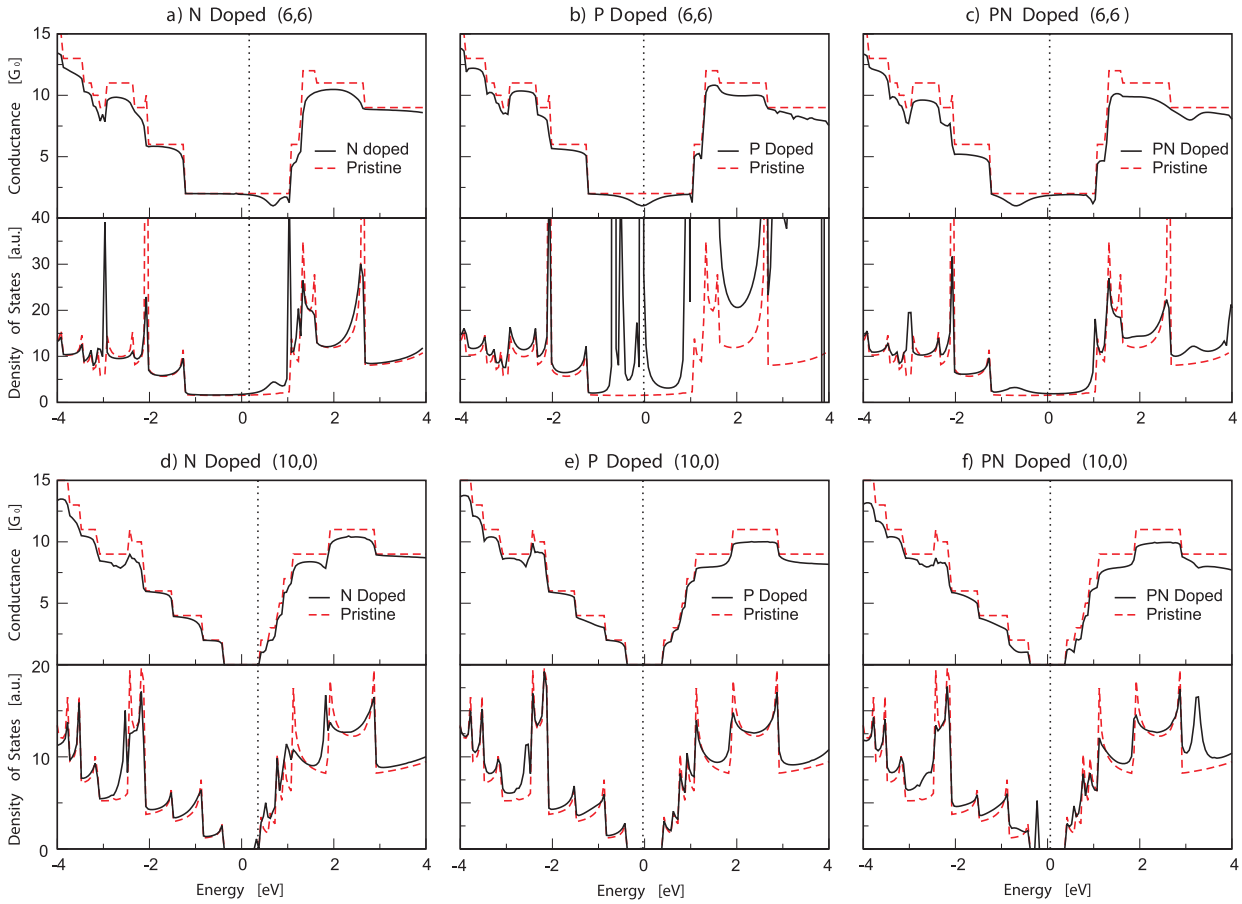

Figure 5. Conductance and density of states plots for doped (6,6) (top) and (10,0) (bottom) carbon nanotubes, compared with pristine nanotube values: (a,d) nitrogen doped, (b,e) phosphorus doped, and (c,f) phosphorus−nitrogen doped nanotubes. Localized states cause scattering and hence a reduction of the conductance for energies close to them in metallic armchair nanotubes. For semiconducting zigzag nanotubes, only nitrogen affects the conductance by shifting the Fermi energy and turning the tube into an *n*-type semiconductor.

trigonal pyramidal coordination, thus creating a localized state related to the extra electron (compared to C) when bonded to a graphitic network. This localized state appears as a nearly nondispersive state, that is, a flat band in the band structure, as seen in Figure 3d,i. Because of their localized nature, these phosphorus-related states have a very long lifetime, do not contribute with electrons to the conduction bands, and therefore they do not affect the semiconducting or metallic character of the nanotubes. These states are also projected as a set of sharp peaks in the electronic density of states at the Fermi level, as shown in Supporting Information, Figure 1. Note that the splitting in two bands observed for the P-doped zigzag nanotube corresponds to the spin up and spin down configurations.[15]

For PN-doped nanotubes, two states are created near the Fermi energy, as observed in Figure 3e,j. For the semiconducting zigzag nanotube (Figure 3j), these states have a low dispersion and reduce the bandgap to half that of the corresponding pristine nanotube, from *ca.* 0.8 eV for pristine (10,0) to *ca.* 0.38 eV for PN-doped nanotube (Figure 3e). The breaking of symmetries in nanotubes due to the presence of dopants is observed in all cases as a loss of degeneracy in the energy bands, and the Van Hove singularities observed in the density of states of pristine nanotubes are smeared (Figure S1).

In Figure 4, a comparison of the amplitude of the wave functions of both nitrogen and phosphorus induced states is shown for metallic (6,6) carbon nanotubes. The plots correspond to the isosurface with a

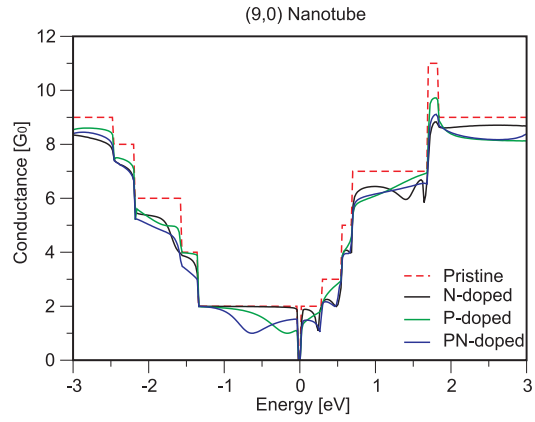

Figure 6. Conductance for a zigzag (9,0) quasi-metallic SWNT with different substitutional doping atoms. It is observed that the behavior is similar to that of the (6,6) armchair case, with the exception of a secondary gap located at the Fermi level of the pristine SWNT.

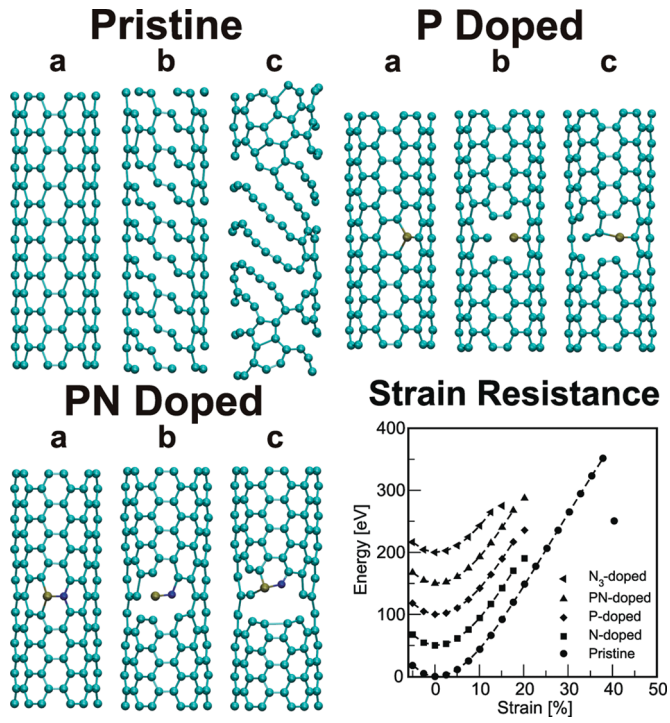

Figure 7. Breaking mechanisms for pristine, P-, and PN-doped carbon nanotubes when subject to strain, showing the tearing process starting at doping sites. For detailed sequences of fracture see Supporting Information, Figure S2. Energy *vs* strain curves (bottom-right) show that doped nanotubes have a resistance to strain at fracture which is half of the pristine tubes. Curves are displayed by increments of 50 eV in the energy scale.

value of 0.05 $Å^{-3/2}$ evaluated at the Γ-point. For the nitrogen-doped case, it corresponds to the states located at the bottom of the conduction band, displaying a strong hybridization with the nitrogen orbitals. For phosphorus, the plot corresponds to the half-filled flat band localized at the Fermi Energy. From the relative degree of localization, as well as the nearly nondispersive band illustrated in Figure 3, it is evident that the electron is strongly bound to the phosphorus atom. In addition, Mulliken population analysis suggests that the P atom has a charge of 5.25 e^-, compared to nitrogen which has 4.39 e^-. The local charge caused by phosphorus atoms is different than nitrogen in the sense that it do not cede part of its charge to the nanotube, hence the nanotube is less negative in the surrounding areas of a phosphorus atom than it is for a nitrogen atom. Such changes in the charge distribution caused by doping with nitrogen can be detected by Raman spectroscopy.[17] Incidentally, the observed difference in the shape of the G′ peak of the Raman spectra of phosphorus-doped SWNT lends strong support to our findings.[15]

For the PN-doped case, two states arise from the dopant atoms, the top valence and the bottom conduction bands. The first state exhibits a strong localization (although not as much as the phosphorus doped case), while the second state has a better mixing with the π-electron system of the carbon network.

The characterization and understanding of the quantum transport properties of the doped nanotubes is fundamental toward their practical use in applications such as components of nanoelectronic devices. The effects of the nitrogen dopant atoms on the electron transport properties of a metallic (6,6) nanotube were found to be consistent with previous reports.[18,19] In particular, there is a reduction of the quantum conductance for energies close to those of the quasibound states associated with the nitrogen atom, slightly above the Fermi Energy, at 0.69 eV, and a second reduction before the first Van Hove singularity, at 1.03 eV, as illustrated in Figure 5a. This is explained by the difference in scattering for the incoming wave function components when the nanotube symmetry is broken by the nitrogen atom. For the zigzag nitrogen-doped nanotube (Figure 5d), the shift in the Fermi energy to the bottom of the conduction bands causes the nanotubes to behave as an *n*-type semiconductor, with a nonzero conductance for positive energies and no conductance for negative energies.

For the armchair phosphorus-doped nanotube (Figure 5b) the highly localized state in the Fermi energy behaves as a scatterer, and the conductance of the armchair (6,6) nanotube is reduced from 2 to 1 G_0, similar to the case of nitrogen's quasibound states. In this case, the symmetry is also lost after the insertion of the phosphorus atom. The PN-doped nanotube has two states that arise from the phosphorus and nitrogen atom bonding to the nanotube, one above and one below the Fermi energy. These states are also reflected as dips in the conductance located at -0.7 and 0.98 eV, as illustrated in Figure 5c.

The conductance for the phosphorus- and phosphorus−nitrogen-doped zigzag nanotubes were not affected by the localized states in the vicinity of the Fermi energy, as indicated in Figure 5e,f. The spatial distribution of these states, which are normal to the nanotube surface, and their strong binding to the phosphorus atom resulted in localized states with infinite lifetime, even after the nanotubes were connected to the semi-infinite nanotube leads. In other words, the zigzag semiconductive nanotubes remain as such, with some changes for energies higher than 1.2 eV, due to the loss of symmetry in the higher energy bands and the smearing of van Hove singularities. The backscattering efficiency of charge transmission in PN-doped nanotubes appear to be much weaker for positive voltages than in N-doped nanotubes, owing to a shallower impurity potential well that weakly traps the induced quasi-bound states, similar to the effect of potassium doping.[20]

The effects of doping on (9,0) metallic zigzag nanotubes were also studied, and is shown in Figure 6. Previously it was observed that the conductance of zigzag quasi-metallic nanotubes is more susceptible to mechanical deformations.[21] As can be seen from Figure 6

TABLE 3. Young Modulus for (6,6) Armchair Nanotubes for Different Dopings. Y_S is calculated According to Hernandez *et al.*[26] and Y is Calculated Using a Wall Thickness of $\delta R = 0.34$ nm

system	Y_S [TPa nm]	Y [TPa]
pristine	0.372394	1.095
N-doped	0.349029	1.027
P-doped	0.345170	1.015
PN-doped	0.341981	1.006
N_3-doped	0.334784	0.985

there are dips in the conductance due to the bound and quasibound states in the doped nanotubes. Overall, the results are similar to those of (6,6) armchair nanotubes, with the exception of the secondary gap of nonarmchair metallic nanotubes,[22,23] present at the Fermi energy of the leads.

The mechanical properties of carbon nanotubes have been of tremendous interest as they have been demonstrated to exhibit incredible axial strength/weight. It was recently shown that avoiding the defects induced by purification steps, unpurified MWCNT displayed a fracture strength which is close to 80% of the theoretical expectation for a defect-free nanotube.[24] In this sense, an investigation of the effects of substitutional doping on the intrinsic mechanical properties of nanotubes is fundamentally important in order to understand how their mechanical performance might be altered. Figure 7 shows the energy−strain curves obtained from the electronic structure calculations for evaluating the fracture strength of pristine and the doped nanotubes, while the stress−strain curves are shown in Supporting Information S3. For all substitutionally doped nanotubes there is a 50% reduced strain at fracture, whereas for the N_3 pyridinic-like defect, the reduction is even greater. In the pristine case, the nanotube can resist a strain of *ca.* 40% elongation before C−C bonds begin to break in several places, leading to a destruction of the hexagonal network and finally creating pentagons and Stone−Wales defects to release some of the lattice stress. In the N, P, and PN-doped cases, the fracture process starts at half the strain, *ca.* 20% elongation, due to the lower hexagon deformation energy. The fracturing process begins with the breaking of the C-dopant bond, but, instead of stress release from lattice reconstruction or reorganization, it is followed by a "tearing" process that continues to the neighboring C−C bonds. For N_3 doping, the stress is released at even lower strains, *ca.* 15% elongation. In this case the breaking occurs at the highly strained C−C bonds between the first and second neighbors of the nitrogen atoms, followed by the tearing of the nanotube.

Although there are major changes in the elasticity of doped nanotubes, it is also observed from Figure 7 that the Young modulus of doped nanotubes (the second derivative of the energy with respect to strain at the equilibrium position) should not be largely affected. Coincident with the findings of Hernández *et al.*,[25] we found that the Young modulus for doped nanotubes is not affected as much as its resistance to strain. In Table 3 we present the calculated young moduli for pristine and doped SWNT, as proposed by Hernández in a previous work.[26] For the pristine case, we have excellent agreement with the result of ref, 25 (0.371 *vs* 0.372 TPa nm). It is observed that substitutional doping causes a reduction of *ca.* 7−8%, probably due to weaker C-dopant bonds. It is also observed that the greater reduction is for N_3 doping, with a 10% reduction, probably due to the structural and bonding changes at the doping site. In the third column we present the Young moduli calculated for a wall thickness of $\delta R = 0.34$ nm. Higher doping densities are expected to further deviate from the defect-free Young modulus and also to further decrease the strain at fracture.

CONCLUSIONS

In this paper we have presented results that rationalize the effects of both phosphorus and heteroatomic phosphorus−nitrogen in carbon nanotubes and why these systems are thermodynamically stable, as recently reported for PN-doped multiwalled carbon nanotubes[14] and P-doped SWNT.[15] The estimation of the defect formation energy shows that, although they have high formation energies (ca. 5 eV for one defect in 200 atoms, $\sim$ 0.5%) these are comparable to the pyridinic N_3 defects. Analysis of the relaxed structures confirms that phosphorus maintains a sp^3 hybridization, and bonds to the carbon atoms with tetrahedral orbitals, inducing structural strain in the carbon network in order to accommodate the longer P−C bonds and the larger sized P ion. Total energy calculations confirmed that curvature helps to reduce the structural strain caused by the phosphorus, and that the P−N defect is energetically more stable than phosphorus alone.

The electronic band structure displays the presence of localized (P) and semilocalized (PN) states around the doping atoms. In contrast to nitrogen, these states do not modify the intrinsic nanotube metallicity, and therefore semiconducting nanotubes remain so regardless of the doping. Electronic transport calculations on pristine, N-, P- and PN-doped nanotubes clarified the different effects of the dopants on their conductance. The calculation of the quantum conductance showed that zigzag phosphorus doped nanotubes do not modify the intrinsic semiconducting behavior, opposed to that observed for N-doped nanotubes.[18] Phosphorus and PN doping in a (10,0) nanotube only create bound and quasibound states around the phosphorus atom, that are dispersionless (represented by flat bands in the band diagram), and projected as sharp peaks in the density of states. These states are normal to the nanotube surface and do not contribute

to the electronic transport in semiconducting nanotubes, while in the case of a metallic nanotube, these states behave as scatterers, creating dips in the conductance.

From the study of the strain resistance of doped nanotubes we conclude that the main difference between the doped and pristine nanotubes originates from the lower hexagon deformation energy caused by the substitutional dopant atoms and from the lack of lattice reorganization/reconstruction. While there is clearly a degradation of the elastic properties, the doped nanotubes offer other distinct advantages. For example, the dopant site of the P nanotubes presents highly localized bound states that by their nature will be very reactive and should strongly bind to molecules (exohedral or endohedral), thus forming considerably enhanced interfacial interactions that should be useful for composite materials fabrication. These properties should also be very useful for fast response and ultrasensitive sensors operating at the molecular level.

METHODS

To investigate the effects of substitutional doping on the electronic and mechanical properties of carbon nanotubes, three different systems were explored: graphene, a (10,0) semiconducting zigzag nanotube, and a (6,6) armchair metallic nanotube. Doping was achieved by direct substitution of carbon atoms with nitrogen and/or phosphorus. Pyridinic-like doping was modeled by creating a vacancy and replacing its first three neighbors with nitrogen atoms. In all cases, the supercell is large enough to ensure that doping atoms do not interact with their periodic images. To that end, 5 unit cells of zigzag nanotubes, 8 unit cells of armchair systems, and a 7 × 7 graphene supercell were carefully chosen, while nanotubes were kept at a lateral distance of a minimum of 10 Å. To calculate the quantum transport properties of the doped systems, a finite section of carbon nanotube containing a doping site was connected to pristine semi-infinite carbon nanotube leads of the same chirality.

The electronic structure of phosphorus- and nitrogen-doped carbon nanotubes has been calculated using the SIESTA code,[27] which was chosen in order to reduce the computational cost due to the relatively large size of the systems studied (~200 atoms), while still retaining the accuracy provided by first-principles techniques. The SIESTA code implements the Kohn−Sham self-consistent density functional method[28,29] on periodic systems using a linear combination of numerical pseudoatomic orbitals as described by Junquera *et al.*[30] The basis size selected was double-ζ with single polarization. The local spin density approximation (LSDA) was chosen for the exchange and correlation potential, in the Ceperley−Alder parametrization of the Perdew and Zunger implementation.[31,32] Norm-conserving Troullier−Martins pseudopotentials in the Kleinman−Bylander nonlocal form were used to represent the core electrons.[33,34] All the models were relaxed by conjugate gradient minimization until the maximum force was less than 0.02 eV/Å. The density of the real space grid used for the intergration of potential and charge is equivalent to that of a plane wave cutoff energy of 150 Ry. The Brillouin zone was sampled by using 8 k-points for nanotubes, and an 8 × 8 Monkhorst−Pack *k*-point grid for graphene.

To investigate on the thermal stability of the nanotubes, molecular dynamics simulations were performed using a Nosé thermostat[35] set at 1000 K for a period of 1 ps, using integration steps of 1 fs. The tensile strength was determined by imposing a deformation in the nanotube axial direction using a series of coordinate rescaling and structure optimization steps. The electronic transport properties were calculated using the Landauer formalism[36,37] and the surface Green functions matching method.[38,39]

Acknowledgment. Authors are grateful to D. Ramirez, G. Ramirez, and G. Pérez-Assaf for technical assistance. E.C.-S., F.L.-U., E.M.-S., M.T., and H.T. acknowledge financial support from CONACYT-Mexico Grants: 56787 (Laboratory for Nanoscience and Nanotechnology Research-LINAN), 45772 (MT), 58899-Inter American Collaboration (MT), 2004-01-013/SALUD-CONACYT (MT), 45762 (HT), Fondo Mixto de San Luis Potosí 63001 S-3908 (MT), Fondo Mixto de San Luis Potosí 63072 S-3909 (HT), 60218-F1 (FLU), 48300 (EMS), as well as for Ph.D. Scolarship (E.C.-S.). J.-C.C. acknowledges financial supports from the FNRS of Belgium, the Belgian Program on Interuniversity Attraction Poles (PAI6) on "Quantum Effects in Clusters and Nanowires", and the ARC sponsored by the Communauté Française de Belgique. E.C.-S., B.G.S. and V.M. acknowledge support by the Division of Materials Science and Engineering, U.S. Department of Energy; and by the Center for Nanophase Materials Sciences (CNMS), sponsored by the Division of Scientific User Facilities, U.S. Department of Energy. Computations were performed using the resources of the ORNL institutional cluster and also from the National Energy Research Scientific Computing Center at LBNL.

Supporting Information Available: Density of states for doped (6,6) and (10,0) CNTs; detailed breaking mechanism of doped (6,6) CNTs under strain; and stress *vs* strain curved for doped (6,6) CNTs. This material is available free of charge *via* the Internet at http://pubs.acs.org.

REFERENCES AND NOTES

1. Oberlin, A.; Endo, M.; Koyama, T. Filamentous Growth of Carbon through Benzene Decomposition. *J. Cryst. Growth* **1976**, *32*, 335–349.
2. Iijima, S. Helical Microtubules of Graphitic Carbon. *Nature* **1991**, *354*, 56–58.
3. Saito, R.; Fujita, M.; Dresselhaus, G.; Dresselhaus, M. S. Electronic Structure of Graphene Tubules Based on C60. *Phys. Rev. B* **1992**, *46*, 1804–1811.
4. Hamada, N.; Sawada, S.; Oshiyama, A. New One-Dimensional Conductors: Graphitic Microtubules. *Phys. Rev. Lett.* **1992**, *68*, 1579–1581.
5. Tans, S. J.; Verschueren, A. R. M.; Dekker, C. Room-Temperature Transistor Based on a Single Carbon Nanotube. *Nature* **1998**, *393*, 49–52.
6. Ajayan, P. M.; Stephan, O.; Colliex, C.; Trauth, D. Aligned Carbon Nanotube Arrays Formed by Cutting a Polymer Resin-Nanotube Composite. *Science* **1994**, *265*, 1212–1214.
7. Charlier, J. C.; Terrones, M.; Baxendale, M.; Meunier, V.; Zacharia, T.; Rupesinghe, N. L.; Hsu, W. K.; Grobert, N.; Terrones, H.; Amaratunga, G. A. J. Enhanced Electron Field Emission in B-Doped Carbon Nanotubes. *Nano Lett.* **2002**, *2*, 1191–1195.
8. Gong, K. P.; Du, F.; Xia, Z. H.; Durstock, M.; Dai, L. M. Nitrogen-Doped Carbon Nanotube Arrays with High Electrocatalytic Activity for Oxygen Reduction. *Science* **2009**, *323*, 760–764.
9. Zamudio, A.; Elias, A. L.; Rodriguez-Manzo, J. A.; Lopez-Urias, F.; Rodriguez-Gattorno, G.; Lupo, F.; Ruhle, M.; Smith, D. J.; Terrones, H.; Diaz, D.; Terrones, M. Efficient Anchoring of Silver Nanoparticles on N-Doped Carbon Nanotubes. *Small* **2006**, *2*, 346–350.
10. Jiang, K. Y.; Eitan, A.; Schadler, L. S.; Ajayan, P. M.; Siegel, R. W.; Grobert, N.; Mayne, M.; Reyes-Reyes, M.; Terrones, H.; Terrones, M. Selective Attachment of Gold Nanoparticles to Nitrogen-Doped Carbon Nanotubes. *Nano Lett.* **2003**, *3*, 275–277.

11. Jiang, K. Y.; Schadler, L. S.; Siegel, R. W.; Zhang, X. J.; Zhang, H. F.; Terrones, M. Protein Immobilization on Carbon Nanotubes *via* a Two-Step Process of Diimide-Activated Amidation. *J. Mater. Chem.* **2004**, *14*, 37–39.
12. Terrones, M.; Souza, A. G.; Rao, A. M. Doped Carbon Canotubes: Synthesis, Characterization, and Applications. *Top. Appl. Phys.* **2008**, *111*, 531–566.
13. Terrones, M.; Jorio, A.; Endo, M.; Rao, A. M.; Kim, Y. A.; Hayashi, T.; Terrones, H.; Charlier, J. C.; Dresselhaus, G.; Dresselhaus, M. S. New Direction in Nanotube Science. *Mater. Today* **2004**, *7*, 30–45.
14. Cruz-Silva, E.; Cullen, D. A.; Gu, L.; Romo-Herrera, J. M.; Munoz-Sandoval, E.; Lopez-Urias, F.; Sumpter, B. G.; Meunier, V.; Charlier, J. C.; Smith, D. J.; *et al.* Heterodoped Nanotubes: Theory, Synthesis, and Characterization of Phosphorus-Nitrogen Doped Multiwalled Carbon Nanotubes. *ACS Nano* **2008**, *2*, 441–448.
15. Maciel, I. O.; Campos-Delgado, J.; Cruz-Silva, E.; Pimenta, M. A.; Sumpter, B. G.; Meunier, V.; Lopez-Urias, F.; Munoz-Sandoval, E.; Terrones, H. ; Terrones, M.; Jorio, A. , Synthesis, Electronic Structure, and Raman Scattering of Phosphorus-Doped Single-Wall Carbon Nanotubes. Nano Lett. **2009**, *9*, 2267−2272.
16. Sumpter, B. G.; Meunier, V.; Romo-Herrera, J. M.; Cruz-Silva, E.; Cullen, D. A.; Terrones, H.; Smith, D. J.; Terrones, M. Nitrogen-Mediated Carbon Nanotube Growth: Diameter Reduction, Metallicity, Bundle Dispersability, and Bamboo-like Structure Formation. *ACS Nano* **2007**, *1*, 369–375.
17. Maciel, I. O.; Anderson, N.; Pimenta, M. A.; Hartschuh, A.; Qian, H. H.; Terrones, M.; Terrones, H.; Campos-Delgado, J.; Rao, A. M.; Novotny, L.; Jorio, A. Electron and Phonon Renormalization Near Charged Defects in Carbon Nanotubes. *Nat. Mater.* **2008**, *7*, 878–883.
18. Choi, H. J.; Ihm, J.; Louie, S. G.; Cohen, M. L. Defects, Quasibound States, and Quantum Conductance in Metallic Carbon Nanotubes. *Phys. Rev. Lett.* **2000**, *84*, 2917–2920.
19. Latil, S.; Roche, S.; Mayou, D.; Charlier, J. C. Mesoscopic Transport in Chemically Doped Carbon Nanotubes. *Phys. Rev. Lett.* **2004**, *92*, 256805.
20. Adessi, C.; Roche, S.; Blase, X. Reduced Backscattering in Potassium-Doped Nanotubes: *Ab Initio* and Semiempirical Simulations. *Phys. Rev. B* **2006**, *73*, 125414.
21. Maiti, A.; Svizhenko, A.; Anantram, M. P. Electronic Transport through Carbon Nanotubes: Effects of Structural Deformation and Tube Chirality. *Phys. Rev. Lett.* **2002**, *88*, 126805.
22. Blase, X.; Benedict, L. X. ; Shirley, E. L.; Louie, S. G. Hybridization Effects and Metallicity in Small Radius Carbon Nanotubes. *Phys. Rev. Lett.* **1994**, *72*, 1878–1881.
23. Kane, C. L.; Mele, E. J. Size, Shape, and Low Energy Electronic Structure of Carbon Nanotubes. *Phys. Rev. Lett.* **1997**, *78*, 1932–1935.
24. Peng, B.; Locascio, M.; Zapol, P.; Li, S. Y.; Mielke, S. L.; Schatz, G. C.; Espinosa, H. D. Measurements of Near-Ultimate Strength for Multiwalled Carbon Nanotubes and Irradiation-Induced Crosslinking Improvements. *Nat. Nanotechnol.* **2008**, *3*, 626–631.
25. Hernandez, E.; Goze, C.; Bernier, P.; Rubio, A. Elastic Properties of Single-Wall Nanotubes. *Appl. Phys. A* **1999**, *68*, 287–292.
26. Hernandez, E.; Goze, C.; Bernier, P.; Rubio, A. Elastic Properties of C and $B_xC_yN_z$ Composite Nanotubes. *Phys. Rev. Lett.* **1998**, *80*, 4502–4505.
27. Soler, J. M.; Artacho, E.; Gale, J. D.; Garcia, A.; Junquera, J.; Ordejon, P.; Sanchez-Portal, D. The SIESTA Method for *ab Initio* Order-N Materials Simulation. *J. Phys.: Condens. Matter* **2002**, *14*, 2745–2779.
28. Hohenberg, P.; Kohn, W. Inhomogeneous Electron Gas. *Phys. Rev.* **1964**, *136*, B864−B871.
29. Kohn, W.; Sham, L. J. Self-Consistent Equations Including Exchange and Correlation Effects. *Phys. Rev.* **1965**, *140*, A1133−A1138.
30. Junquera, J.; Paz, O.; Sanchez-Portal, D.; Artacho, E. Numerical Atomic Orbitals for Linear-Scaling Calculations. *Phys. Rev. B* **2001**, *64*, 235111.
31. Ceperley, D. M.; Alder, B. J. Ground-State of the Electron-Gas by a Stochastic Method. *Phys. Rev. Lett.* **1980**, *45*, 566–569.
32. Perdew, J. P.; Zunger, A. Self-Interaction Correction to Density-Functional Approximations for Many-Electron Systems. *Phys. Rev. B* **1981**, *23*, 5048–5079.
33. Troullier, N.; Martins, J. L. Efficient Pseudopotentials for Plane-Wave Calculations. *Phys. Rev. B* **1991**, *43*, 1993–2006.
34. Kleinman, L.; Bylander, D. M. Efficacious Form for Model Pseudopotentials. *Phys. Rev. Lett.* **1982**, *48*, 1425–1428.
35. Nose, S. A Unified Formulation of the Constant Temperature Molecular Dynamics Methods. *J. Chem. Phys.* **1984**, *81*, 511–519.
36. Landauer, R. Electrical Resistance of Disordered One-Dimensional Lattices. *Philos. Mag.* **1970**, *21*, 863–867.
37. Datta, S. *Electronic Transport in Mesoscopic Systems;* Cambridge University Press: New York, 1995.
38. Nardelli, M. B. Electronic Transport in Extended Systems: Application to Carbon Nanotubes. *Phys. Rev. B* **1999**, *60*, 7828–7833.
39. Meunier, V.; Sumpter, B. G. Amphoteric Doping of Carbon Nanotubes by Encapsultation of Organic Molecules: Electronic Properties and Quantum Conductance. *J. Chem. Phys.* **2005**, *123*, 024705.